

Luminescence properties of non-stoichiometric lithium niobate crystals of various composition and genesis (review)

© M.V. Smirnov, N.V. Sidorov, M.N. Palatnikov

Tananaev Institute of Chemistry Subdivision of the Federal Research Centre „Kola Science Centre of the Russian Academy of Sciences“, Apatity, Russia

✉ e-mail: m.smirnov@ksc.ru

Received June 09, 2021

Revised September 20, 2021

Accepted September 24, 2021

A brief review of the features of the defect structure and studies of the luminescent properties of nonlinear optical lithium niobate crystals of various compositions and genesis was given. It was established that the electron-hole pair $\text{Nb}_{\text{Nb}}^{4+}-\text{O}^-$ in the oxygen-octahedral cluster NbO_6 emitted in the short-wavelength region of the visible spectrum (400–500 nm), while point defects (V_{Li} and $\text{Nb}_{\text{Nb}}^{4+}-\text{Nb}_{\text{Li}}^{4+}$ bipolarons) — in the long-wavelength region (500–620 nm). At the ratio of $\text{Li}/\text{Nb} \approx 1$ the luminescence was extinguished in the visible region of the spectrum due to decreasing the intrinsic luminescence centers. It was shown that the presence of polaron luminescence in the near-IR region (700–1050 nm) was due to the small polarons $\text{Nb}_{\text{Li}}^{4+}$ and impurity ions Cr^{3+} localized in lithium and niobium octahedra. The energy transfer between the luminescence centers in the visible and near-IR spectral regions was detected. Moreover, luminescence in near-IR regions was dominant. Doping of LiNbO_3 crystals with zinc and magnesium at $\text{ZnO} < 4.46 \text{ mol.}\%$ and $\text{MgO} < 5.29 \text{ mol.}\%$ led to decreasing luminescence of intrinsic defects (V_{Li} , $\text{Nb}_{\text{Nb}}^{4+}-\text{Nb}_{\text{Li}}^{4+}$). However, there was an increase of the contribution of the short-wave spectrum component at higher dopant concentrations because of the introduction of Zn and Mg into the origin positions of Nb ions.

Keywords: lithium niobate single crystal, point defects, luminescence, luminescence centers.

DOI: 10.21883/EOS.2022.01.53002.14-21

Introduction

Lithium niobate single crystal (LiNbO_3) is an important functional optical material widely used in telecommunication equipment, integrated optics and laser technology. Lithium niobate is a deeply defective oxygen-octahedral phase of variable composition with a wide region of homogeneity in the phase diagram, which makes it possible to change the stoichiometry of the crystal ($[\text{Li}]/[\text{Nb}]$ ratio), as well as to introduce dopants into the structure, thereby changing the defect state and physical characteristics of the crystal [1,2]. Nominally pure LiNbO_3 crystals of congruent ($[\text{Li}]/[\text{Nb}] = 0.946$) and stoichiometric compositions ($[\text{Li}]/[\text{Nb}] = 1$) are distinguished by significantly different coercive field strengths equal to ~ 21 and $\sim 5 \text{ kV/mm}$, respectively. But stoichiometric crystals grown from a melt with 58.6 mol% Li_2O are characterized by a much stronger photorefractive effect [3–6]. Doping of crystals with magnesium or zinc makes it possible to reduce the effect of photorefractive and reduce the magnitude of the coercive field (to 4.6 and 1.4 kV/mm for Mg and Zn, respectively [7,8]), which is important for creating materials converting the laser radiation on periodically polarized micron and submicron sized domains [9–14]. In this case, the limiting factor is the presence of luminescence.

An ideal stoichiometric crystal has a transparency window in the region of 320–5000 nm [15]. An ideal stoichiometric

crystal should not contain luminescence centers. However, real LiNbO_3 crystals always contain point defects Nb_{Li} (niobium cations located in the positions of lithium cations of the ideal structure). The concentration of such defects is especially high in crystals grown from a melt with an excess of niobium ($[\text{Li}]/[\text{Nb}] < 1$). Thus, in a congruent crystal, the concentration of Nb_{Li} point defects is $\approx 6 \text{ at}\%$ [16] or 1 mol% [17]. The presence of Nb_{Li} defects due to the conservation of charge electrical neutrality of the crystal, in its turn, leads to the formation of a full spectrum of point and complex defects in the crystal, they act as traps of holes and electrons. The role of defects in the form of shallow and deep electron traps in the band gap, as well as defects that change the polarizability of oxygen-octahedral clusters MeO_6 ($\text{Me}=\text{Li}^+$, Nb^{5+} , doping cation) and the ordering of the structural units of the cation sublattice along the polar axis is decisive in the formation of practically significant physical properties, in particular, luminescence, photorefractive, spontaneous polarization, and coercive field. Therefore, to create materials based on LiNbO_3 crystal for generating and converting laser radiation, in addition to reducing the photorefractive properties, it is necessary to reduce the number of defects in the crystal which determine the spontaneous radiative recombination in the optical region of the spectrum.

In this paper, we briefly review the studies of the defect structure of lithium niobate crystals of various compositions

and genesis in order to establish the effect of defects of various types on the luminescence characteristics of nominally pure LiNbO_3 crystals, as well as crystals doped with magnesium and zinc. The review deals only with the problems of radiative recombination of the luminescence centers of the LiNbO_3 crystal matrix, but does not address intraconfigurational $4f^n-4f^n$ transitions of rare-earth elements (REE) and the accompanying luminescence mechanisms (up-conversion, energy transfer „matrix-REE“ or „REE-REE“, non-linear optical amplification), which are covered in detail in the papers [18–21]. Emphasis is placed on research and analysis of literature data on the intrinsic luminescence of the lithium niobate crystal matrix depending on the stoichiometry, type of dopant and its concentration, annealing conditions, etc. and comparing them with our experimental data on the photoluminescence of LiNbO_3 crystals of different composition and genesis. The article relates to a material science. The purpose of the paper is not to interpret the luminescence spectra (this has already been done in the other papers [19,20,22]), but to study the luminescence of crystal matrix in order to obtain optical materials for converting optical radiation with the lowest possible photoluminescence. The paper consists of three Sections. The first Section describes sample preparation methods and measurement techniques. The second Section presents information about the main point defects formed in LiNbO_3 crystal upon a change in stoichiometry and doping with different concentrations of Mg^{2+} and Zn^{2+} cations. The third Section presents information about the luminescence properties of the investigated LiNbO_3 crystals and characterizes the main luminescence centers of the matrix.

1. Materials and methods

All crystals were grown in air by the Czochralski method of a granular charge of lithium metaniobate, synthesized on the basis of the ICT KSC RAS method [23]. Congruent crystals ($\text{LiNbO}_{3\text{cong}}$) were grown from a congruent melt ($[\text{Li}]/[\text{Nb}] = 0.946$). LiNbO_3 stoichiometric crystals were obtained in two ways: from a melt with 58.6 mol% Li_2O ($\text{LiNbO}_{3\text{st}}$) and by the HTTSSG (high temperature top seeded solution growth) method from melt of congruent composition with addition of alkaline flux $\text{K}_2\text{O} \approx 6.0$ mol% ($\text{LiNbO}_{3\text{st}}:\text{K}_2\text{O}$). LiNbO_3 crystals doped with Zn at concentration of 0.07, 1.19, 2.01, 4.46, 5.50, and 6.50 mol% ZnO and doped with Mg with concentration of 0.19, 1.65, 2.13, 3.02, 5.29, 5.91 mol% were obtained using the method of direct doping of the melt. See details of the growth of LiNbO_3 crystals of different composition and genesis in the papers [2,24]. The concentration of trace amounts of uncontrolled impurities in crystals does not exceed $1 \cdot 10^{-3}$ for Mo, Fe, Ti, Si, Pb, Ni, Cr, Co and $5 \cdot 10^{-4}$ wt% for Al, Cu, Mn, V, Mg, Sn.

The monodomainization of crystals was carried out by high-temperature electrodiffusion annealing with cooling

the samples at a rate of $20^\circ/\text{h}$ in the temperature range of $\sim 1240\text{--}890^\circ\text{C}$ when electrical voltage is applied [23]. The degree of monodomainness was monitored by impedance spectroscopy and by measuring the static piezoelectric modulus ($d_{33\text{st}}$) of the crystal boule. The studied samples, cut from the crystal boule, were rectangular parallelepipeds with dimensions $\sim 8 \times 7 \times 6 \text{ mm}^3$, the edges of which coincided with the directions of the crystallographic axes X, Y, Z (Z is the polar axis of the crystal).

Photoluminescence spectra were measured from surface macrodefects and the bulk of the studied LiNbO_3 crystals using a SOL SL-100M spectrograph with CCD detector FLI ML 1107 BlackIlluminated (Hamamatsu) in two wavelength ranges: 380–800 and 600–1050 nm, under normal conditions. The CCD-matrix in the operating mode was cooled by a Peltier element to -30°C . The width of the entrance slit of the monochromator was 0.25 mm for measurements from the surface of LiNbO_3 crystal and 1.00 mm for measurements from the bulk of the crystals under study. A continuous He–Cd laser ($\lambda_{\text{ex}} = 325 \text{ nm}$, 15 mW) was used as a luminescence excitation source. Each photoluminescence spectrum was normalized to the background signal.

2. Defect structure of LiNbO_3 crystal

The structure of LiNbO_3 crystal of any composition within the homogeneity region is described by a spatial symmetry group $R3c$ with two formula units per lattice cell. The crystal consists of alternating O_6 oxygen octahedrons, each of which is rotated relative to each other by 120° . Two-thirds of the O_6 octahedrons contain Nb and Li ions, while one third of the octahedrons remain vacant, so that a chain $\dots -\text{Nb}-\text{Li}-\square-\text{Nb}-\text{Li}-\square-\text{Nb}-\text{Li}-\square-\dots$ (\square is empty octahedron) is formed along the polar axis of the crystal (Fig. 1). Under normal conditions, a lithium niobate crystal is in ferroelectric phase due to the displacement of Li and Nb ions from the centrosymmetric position relative to the oxygen plane along the direction of the polar axis c by 0.44 and 0.26 Å respectively [1,25].

In nominally pure nonstoichiometric crystals and in doped LiNbO_3 crystals, the distribution of major (Li and Nb) and impurity cations over octahedrons along the polar axis is extremely complex and difficult to model mathematically. This is usually done by full-profile X-ray diffraction analysis (Rietveld method) using vacancy split models [26]. Initially, the authors of the paper [27] proposed a vacancy model that takes into account the simultaneous formation of oxygen and lithium vacancies, $[\text{Li}_{1-2x}\text{V}_{2x}][\text{Nb}][\text{O}_{3-x}\text{V}]$, and as the stoichiometry ($[\text{Li}]/[\text{Nb}]$ ratio) increases, the fraction of such defects decreases. This model is inconsistent with the data of papers [28,29], in which an increase in the crystal density occurs with a decrease in the $[\text{Li}]/[\text{Nb}]$ ratio. In this case, excessive niobium atoms are mainly introduced into the lithium (Nb_{Li})

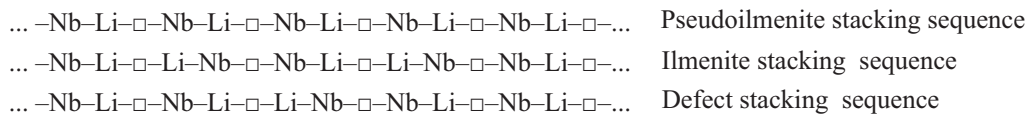


Figure 1. The location of cations along the polar axis c in pseudo-ilmenite and ilmenite structures and the supposed split structure of LiNbO_3 crystal [25,31].

positions, since the dimensions of the lithium octahedron are larger than those of the niobium one. To preserve the electrical neutrality of the crystal, the effective excessive charge of niobium, $4|e|$, where e is the electron charge, is compensated by four lithium vacancies, V_{Li} (the model of lithium vacancies, $[\text{Li}_{1-5x}\text{Nb}_x\text{V}_{4x}][\text{Nb}][\text{O}_3]$) [28]. The model of lithium vacancies agrees well with the data of X-ray diffraction analysis [30]. Besides, the formation of oxygen vacancies is energetically unfavorable [31].

The crystal density increasing with the stoichiometry decreasing can be explained in terms of the formation of niobium vacancies (V_{Nb}). Thus, during careful NMR study of ^{96}Nb [32] of LiNbO_3 crystal another vacancy model was suggested: the niobium vacancy model, $[\text{Li}_{1-5x}\text{Nb}_{5x}][\text{Nb}_{1-4x}\text{V}_{4x}][\text{O}_3]$, in which niobium is in the lithium position and niobium vacancy V_{Nb} forms near it. The model was developed by the authors of the paper [16] on the basis of X-ray diffraction studies of LiNbO_3 crystal.

Comparison of models of lithium and niobium vacancies is presented in the papers [30,31,33,34]. The lithium vacancies model describes the defect structure better according to neutron diffraction and X-ray diffraction data, in contrast to the niobium vacancies model [30] for LiNbO_3 crystals with the ratio $[\text{Li}]/[\text{Nb}] = 0.992, 0.942, 0.887$. With the concentration of Nb ions increasing in the crystal structure of lithium niobate, the Nb^{5+} ions in the main octahedron tend to the centrosymmetric position, while the Li^+ ions, on the contrary, tend to move along the polar axis z from the center of the octahedron to the nearest oxygen plane [30]. Based on calculations of the soft mode frequency and the Curie temperature, the defect structure of the LiNbO_3 crystal is better described in terms of the lithium vacancies model [33]. In addition, computer simulation has shown that the lithium vacancies model is more energetically favorable than the niobium vacancies model [31,34]. However, based on the analysis of the frequency dependence of the $E(\text{TO}_1)$ and $A_1(\text{TO}_{1-4})$ phonons of the crystal lattice on the crystal composition, it was found that the defect structure of LiNbO_3 crystal of different composition can be described in terms of a split model that combines the models of niobium and lithium vacancies, the latter prevails with the congruent composition of $[\text{Li}]/[\text{Nb}] \geq 0.946$ [35].

In the paper [36] the distribution of the main cations (Nb, Li) and vacancies (□) along the polar axis of the LiNbO_3 crystal was studied within the structure of pseudo-ilmenite (Fig. 1). Computer modeling of clusters in the structure of a lithium niobate crystal [31] shows that two modifications of the pseudoilmenite structure are possible

and stable. In this case, the energy of the crystal lattice per lattice cell in the structure of both modifications differs only by 0.3%. In this case, the lattice cell periods increase on average by 2% in comparison with the pseudo-ilmenite structure [37]. In this regard, the authors suppose that the possible simultaneous coexistence of clusters of both modifications in the structure of LiNbO_3 crystal is possible, which makes it possible to expand the existing defect models. The fact of simultaneous coexistence of clusters of two modifications may confirm the presence of „extra“ low-intensity lines (which do not correspond to lattice fundamental vibrations) in the Raman spectroscopy (RSS) [25]. At that, the number of „extra“ lines is approximately equal to the number of lines corresponding to the lattice fundamental vibrations. It was proposed in paper [36] that the presence of V_{Nb} defects in the pseudo-ilmenite structure of LiNbO_3 crystal can be interpreted, as in the ilmenite structure, based on the lithium vacancies model. The authors of the paper [37] state that the weak maximum in the RSS spectrum at 738 cm^{-1} corresponds to a phonon in the ilmenite packing structure of the LiNbO_3 crystal. In the RSS spectrum of $\text{LiNbO}_{3\text{cong}}$ crystal (in contrast to the spectrum of $\text{LiNbO}_{3\text{st}}$) in the 180° scattering geometry in polarizations ((YX), (XY), (YY), (XX)) this maximum appears confidently when the spectra are excited both in the visible and near IR regions [38].

For doped crystals the model of the defect structure and the mechanism by which the dopant enters the crystal lattice will depend on the type and concentration of the dopant. In this case, the dopants entry has a pronounced threshold nature. In certain concentration ranges the physical characteristics (Curie temperature, lattice periods, conductivity, etc.) change step-wise [2,25]. Effect of doping „non-photorefractive“ cations Zn^{2+} , Mg^{2+} etc. on the optical properties and composition homogeneity of LiNbO_3 crystal tends mainly to a change in the order of alternation along the polar axis of the main cations (Li^+ and Nb^{5+}), the concentration of trace amounts of impurity cations and intrinsic point and complex defects. At the same time, a significant technological advantage of $\text{LiNbO}_3:\text{Zn}$ crystals is that with a change in the Zn concentration in the crystal, a smoother change in the defect state and its physical characteristics occurs than with a change in the concentration of Mg [2]. In this paper the description of the defect structure in doped $\text{LiNbO}_3:\text{Zn}$ and $\text{LiNbO}_3:\text{Mg}$ crystals will be based on the model of lithium vacancies, since it plays a dominant role in comparison with the model of niobium vacancies.

Due to the larger size of the lithium octahedron relative to the niobium octahedron the distance between the Li^+ ions and the nearest O^- ions is 2.072 and 2.273 Å, while for the Nb^{5+} ion — 1.885 and 2.102 Å [39]. Correspondingly, the mechanism of the doping mixture of zinc and magnesium at a low concentration entry into LiNbO_3 crystal lattice begins predominantly with the incorporation into lithium positions. In the case of doping with low concentrations of Mg and Zn the entry mechanism is determined by the incorporation to lithium positions with a simultaneous decrease in the number of Nb_{Li} defects [40]. Complete displacement of Nb ions by Mg ions is observed at a concentration of 3 mol% [37]. At higher concentrations, Mg enters the structure in both lithium and niobium positions [40]. If stacking faults are considered, then Mg concentration increasing should be accompanied by intensity decreasing in the RSS spectrum of line with a frequency of 738 cm^{-1} . The complete disappearance of this line from the spectrum is observed in the region between 2.0 and 4.0 mol% of MgO. Based on RSS data, the authors [37] conclude that this corresponds to the complete absence of clusters with the ilmenite structure in the structure of the lithium niobate crystal. Similar regularities are observed upon doping with In^{3+} and Ti^{4+} atoms [37]. Due to Zn smoother entry into the crystal lattice of LiNbO_3 , with the concentration increasing several intermediate stages will be observed in comparison with $\text{LiNbO}_3:\text{Mg}$ crystals. At concentrations of $0 < [\text{Zn}] < 2.87\text{ at}\%$, the Nb_{Li} defects and Li are smoothly displaced with slight increase in the number of V_{Li} defects [41,42]. At concentrations of $2.87 < [\text{Zn}] < 5.2\text{ at}\%$ there are no Nb_{Li} and V_{Li} defects, above $[\text{Zn}] > 5.2\text{ at}\%$ zinc incorporation already in niobium positions occurs with the formation of V_{Nb} defects [39,42,43].

Thus, in nominally pure LiNbO_3 crystals and doped $\text{LiNbO}_3:\text{Mg}(\text{Zn})$ crystals the defect structure can be described in terms of vacancy split models, except for the model of oxygen vacancies. The predominant vacancy model is the lithium vacancies model, in which there are four V_{Li} defects per one excessive niobium atom (Nb_{Li} defect). However, it is most expedient to consider the additive action of both vacancy models and take into account the role of not only V_{Li} , but also V_{Nb} , considering the stacking fault of the alternation of basic metal cations along the polar axis c . In doped crystals at low concentrations the dopant (Zn^{2+} , Mg^{2+}) is introduced into the Li positions, at threshold values — into the Nb main positions.

3. Luminescence properties of LiNbO_3 crystal

In modern optical materials science, LiNbO_3 crystals of various compositions and genesis can be used for holographic recording of information, as well as for nonlinear frequency conversion of laser radiation. The possibility of recording the hologram depends directly on the photorefractive properties of the LiNbO_3 crystal. In the process

of recording, charge carriers are photoexcited from deep energy levels (traps), and then under the action of diffusion and drift they move from the region illuminated by laser radiation to the unilluminated region, followed by capture in traps. In this case, a hologram is recorded due to the induction of the space charge field and, accordingly, the optical properties of the crystal change. The problem lies in the hologram reading, as there is repeated exposure to laser radiation, which leads to charge redistribution, and thereby erases the holographic information [44]. A partial solution to the problem of nondestructive optical reading of hologram is, for example, a two-stage recording with intermediate state with a lifetime sufficient to create the necessary population of this level [25,45,46], or reading the hologram in an external magnetic field due to abnormally high Hall photocurrent [47]. On the other hand, the photoinduced change in the refractive indices leads to distortion of the light wave front and disruption of laser radiation generation in solid-state lasers based on lithium niobate crystals doped with rare earth elements [48]. Next, the processes of relaxation of free charge carriers are reviewed from the point of view of studying the luminescent properties of lithium niobate crystals.

According to literary sources [49–52], the luminescence of LiNbO_3 crystal is observed in the visible and near IR regions of the optical spectrum. Spectral distribution of luminescence intensity depends on many factors, such as stoichiometry [52,53], type and concentration of dopant [53–56], annealing conditions [57,58], exposure to ionizing radiation [59,60], places of luminescence excitation [50,61], which changes the mechanisms of defect formation, their distribution in the lattice and the charge state of some transition metals without changing their concentration in the LiNbO_3 crystal, and, as a consequence, the channels of matrix radiative recombination.

Some qualitative conclusions about the luminescence of LiNbO_3 crystals are presented in the paper [49]. It was found that the emission in the near IR spectral region with a maximum at 840 nm ($\Delta\lambda = 200\text{ nm}$) is independent of the crystal orientation relative to the incident radiation (ruby laser, $\lambda_{\text{ex}} = 696\text{ nm}$, excitation occurs from energy impurity levels and dislocations), and the intensity is directly dependent on the length of the crystal [49]. It has been found that as the temperature increases from 294 to 526 K, the luminescence intensity decreases exponentially. The activation energy is correspondingly equal to $E_a = 0.28 \pm 0.03\text{ eV}$. In this case, the width of the maximum does not depend on the increase in temperature. Above $T > 448\text{ K}$ the luminescence becomes very weak. It is assumed that the luminescence centers involved in radiative recombination are also responsible for the photorefractive properties, and the characteristic decay time corresponds to the time during which the photoelectron is recaptured in the trap.

Further development of luminescence studies is given in the paper [62]. The luminescence spectra of the $\text{LiNbO}_3:\text{Eu}^{3+}, \text{Cr}^{3+}$ crystal exhibit two broad maxima at 500 and 820 nm ($\Delta\lambda = 200$ and 150 nm). The nature of the

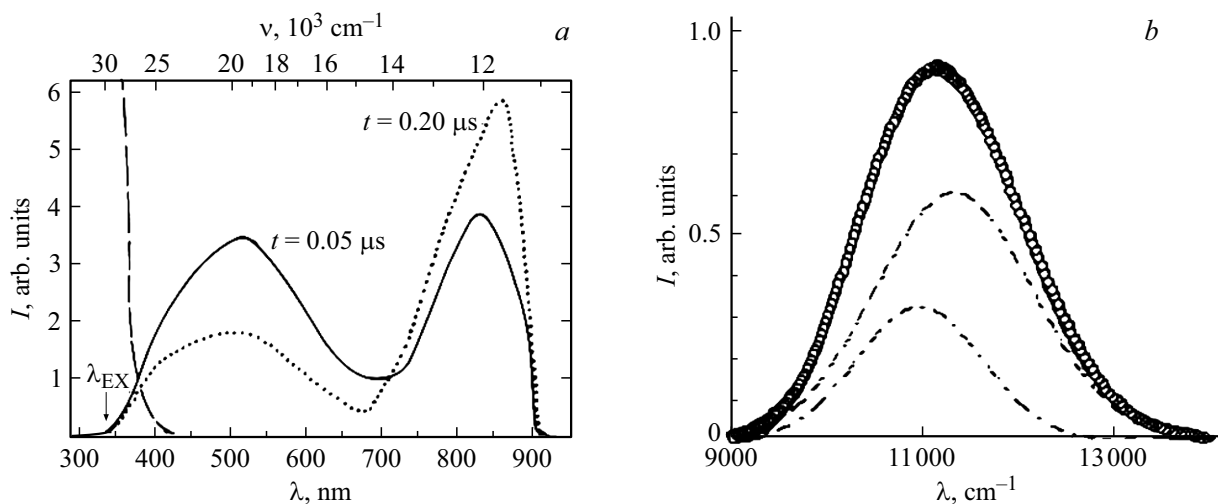


Figure 2. *a* is absorption spectrum (dashed curve) and fluorescence spectra of $\text{LiNbO}_3:\text{Eu}^{3+}, \text{Cr}^{3+}$ crystal exposed to laser radiation (337 nm) for 0.05 and 0.20 μs (solid, dotted curves) at $T = 300 \text{ K}$ [42]; *b* is luminescence spectrum of $\text{LiNbO}_3:\text{Cr}, \text{Mg}$ crystal after decomposition to two Gaussian components: 11363 and 10869 cm^{-1} for Cr_{Li} and Cr_{Nb} [47].

first maximum corresponds to the emission of the matrix, while the nature of the second one is ${}^4T_2-{}^4A_2$ -transitions (*R*-lines) to Cr^{3+} ions. With an increase in the time of exposure to laser radiation (N_2 -laser, $\lambda_{\text{ex}} = 337 \text{ nm}$), energy is transferred between these maxima with a predominance of intensity in the near IR region of the spectrum, while Eu^{3+} ions do not participate in energy transfer [62] (Fig. 2, *a*). Cr^{3+} ions are placed in lithium positions, forming a Cr_{Li} center [55,63,64]. These centers depend on local excitations that create V_{Li} ($\beta\text{-Cr}_{\text{Li}}$), Nb_{Li} ($\alpha\text{-Cr}_{\text{Li}}$), and $\gamma\text{-Cr}_{\text{Li}}$ center has no defects in the coordination environment. Characteristic luminescence in $\text{LiNbO}_3:\text{Cr}$ is observed at 13690, 13620 and 13540 cm^{-1} (730, 734 and 739 nm) for $\beta\text{-Cr}_{\text{Li}}$, $\alpha\text{-Cr}_{\text{Li}}$ centers and 0–0-electron transition [55]. The latter is observed only in the LiNbO_3 crystal, whose composition is close to stoichiometric. In a congruent crystal, the *R*-lines of Cr^{3+} are widened by 2–2.5 times relative to the crystal obtained using VTE (Vapour Transport Equilibrium) technologies [65]. However, the luminescence of Cr^{3+} centers ($E < 13650 \text{ cm}^{-1}$) undergoes thermal quenching up to $T = 60 \text{ K}$ [55]. The paper [63,64] shows a thorough analysis of the kinetic-luminescent characteristics of gradient-activated $\text{LiNbO}_3:\text{Cr}^{3+}:\text{Mg}^{2+}$ crystals (the concentration of Cr^{3+} 0.05 at%) and found that Cr^{3+} optical centers can be incorporated both in lithium positions and niobium positions, at that radiative transitions under normal conditions ($T = 300 \text{ K}$) are observed at 11363 and 10869 cm^{-1} (880 and 920 nm) for Cr_{Li} and Cr_{Nb} (Fig. 2, *b*). Doping with MgO results in a „red“ shift of wide absorption bands ${}^4A_2-{}^4T_2$ and ${}^4A_2-{}^4T_1$ of Cr^{3+} , and increasing the Mg concentration from 1 to 3 at% reduces the absorption of ${}^4A_2-{}^4T_2$ -bands [55,64]. In the luminescence spectrum, in addition to the Cr_{Li} centers the emission bands at 13510 and 13565 cm^{-1} (740 and 737 nm) are observed, the nature of which is associated with Cr_{Nb} centers. The presence of

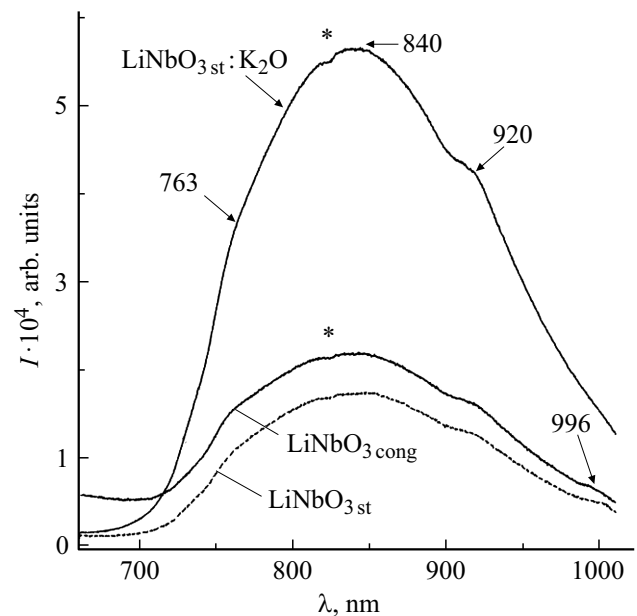


Figure 3. Photoluminescence spectra of nominally pure LiNbO_3 crystals in the near IR region of the spectrum, $\lambda_{\text{ex}} = 325 \text{ nm}$ and $T = 300 \text{ K}$.

Mg_{Li} defect leads to a shift in the luminescence peak of $\alpha\text{-Cr}_{\text{Li}}$ center, which indicates a change in the crystal field (the replacement of Nb_{Li} on Mg_{Li}) [55]. An interesting assumption was made in the paper [64], at a concentration of $[\text{Mg}] > 2 \text{ at\%}$, in addition to the localization of Mg atoms in niobium positions, the radiative recombination of the center Cr_{Nb} is stimulated by introducing Mg atom into the interstice.

Our photoluminescence spectra of nominally pure LiNbO_3 crystals show a similar luminescence halo in the near IR region of the spectrum with more pronounced

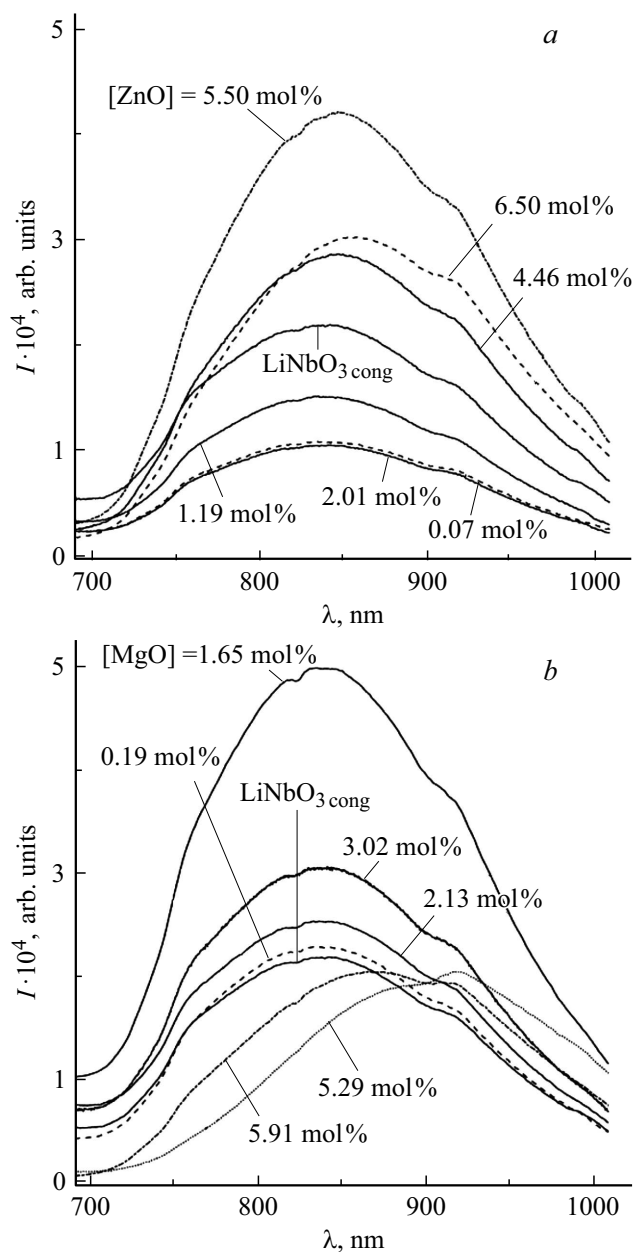


Figure 4. Photoluminescence spectra of $\text{LiNbO}_3\text{:Zn}$ (a) and $\text{LiNbO}_3\text{:Mg}$ (b) crystals in the near IR region of the spectrum, $\lambda_{\text{ex}} = 325 \text{ nm}$ and $T = 300 \text{ K}$.

luminescence maxima at 763, 840, 920, and 996 nm (Fig. 3). Usually, a wide luminescence band with two overlapping maxima at 1.3 and 1.5 eV (954 and 827 nm) [51] is observed in this region. In addition, the dip at 823 nm (*) may indicate energy absorption by other luminescence centers. Similar photoluminescence spectra are obtained in LiNbO_3 crystals doped with Zn or Mg (Fig. 4). It is possible that additional luminescence centers in the form of small-radius polarons, whose luminescence is also in the near IR region of the spectrum, are involved in the process of radiative recombination. In another paper [57] it was shown that the capture of an electron from the conduction

band by Nb_{Li} defect is accompanied by emission in the near IR region with a maximum at 850 nm. In another paper [66] the luminescence peak at 1.57 eV (790 nm) is associated with the polaron luminescence of $\text{Nb}_{\text{Li}}^{4+}$, and its intensity is proportional to the concentration of Nb_{Li} in LiNbO_3 crystal. At the same time, the study of the magnetic circular dichroism of the absorption band at 1.6 eV (776 nm) showed that its nature is related to the small-radius polaron $\text{Nb}_{\text{Li}}^{4+}$ [67]. Indeed, a decrease in the intensity of the maximum at 763 nm (Fig. 3) is observed in the spectrum of LiNbO_3st crystal relative to $\text{LiNbO}_3\text{cong}$, which corresponds to a smaller number of Nb_{Li} point defects in the stoichiometric crystal. The contribution of $\text{Nb}_{\text{Li}}^{4+}$ polaron luminescence to the total luminescent signal decreases during doping by Mg (5.29 and 5.91 mol%) or Zn (0.07–2.01 and 6.50 mol%) of LiNbO_3 crystals (Fig. 4).

Besides, heat treatment in air leads to co-enrichment of the near-surface region of the crystal with Nb_{Li} defects, which increases polaron luminescence [57]. When the surface of $\text{LiNbO}_3\text{:Fe}$ crystal is doped, the polaron luminescence is quenched, since excessive Nb^{5+} cations are forced out of lithium positions [57,66]. At $[\text{Fe}] = 1 \text{ at\%}$ in $\text{LiNbO}_3\text{:Fe}$ crystal the integral intensity of the polaron luminescence of Nb_{Li} drops by 50% [66]. The Fe^{2+} ions represent donor centers, and their characteristic absorption band is observed at 2.66 eV (467 nm), the intensity of which is proportional to the concentration of $[\text{Fe}^{2+}]$ [56,68]. After photoexcitation of Fe^{2+} ions the electron can be recaptured on Fe^{3+} or localized on Nb_{Li} defect with the formation of small-radius polaron, which leads to increased polaron luminescence of Nb_{Li} [56]. However, in the LiNbO_3 crystals under study the Fe^{2+} impurity is found in trace amounts (10^{-3} mol\%), which makes it difficult to analyze its influence on the relaxation of electronic excitations, and its influence is minimum.

By analogy with similar mechanisms of radiative recombination in CaWO_4 and YVO_4 crystals, it can be assumed that the luminescence of LiNbO_3 crystals in the visible range is associated with oxygen-octahedral clusters of NbO_6 . Careful analysis of the EPR data [69] showed that the electrons are localized on the Nb^{5+} ions in the main positions with the formation of small-radius polaron („free polaron“) — $\text{Nb}_{\text{Nb}}^{4+}$, and holes are trapped at acceptor centers, presumably on O^- ions („free hole polaron“). In the process of excitation the electron passes from $2p\text{-O}$ molecular orbital to t_{2g} molecular orbital of the Nb^{5+} ion [62]. The Stokes shift is 15700 cm^{-1} for a maximum at 500 nm [70,71]. In this case, the decay time does not depend on temperature ($T = 14\text{--}300 \text{ K}$) and is equal to $0.22 \mu\text{s}$, which indicates a deep electron trap. The formation of hole traps O^- , which are located near lithium vacancies („bound hole polaron“), is accompanied by increasing of absorption coefficient in the visible region at 2.5 eV (496 nm) [72,73]. At room temperature or under intensive illumination a weak absorption of this trap is observed, which may be due to recombination processes with small-radius polarons [74,75]. In papers [59,76,77]

the electron-hole recombination between $\text{Nb}_{\text{Nb}}^{4+}$ and O^- is observed at 2.82–2.6 eV (440–477 nm).

The study of the photoluminescence spectrum evolution of crystals $\text{LiNbO}_3:\text{Mg}$ ([Mg] = 3 and 7 mol%) in time (time-resolved photoelectron spectroscopy) shows the distribution of the luminescence intensity $I(t, \lambda)$ with a maximum at 2.62 eV (474 nm) in the spectral range from 400 to 650 nm and in the range with a time resolution from 10^{-9} to $6 \cdot 10^{-6}$ s at $T = 150$ K [78]. The authors suppose that photoluminescence at 2.62 eV is the result of polaron recombination of $\text{Nb}_{\text{Nb}}^{4+}$ and O^- . In this case, the decay kinetics of this emission band is described by two exponential functions. For LiNbO_3 crystal with [Mg] = 7 mol% the luminescence duration $\tau_1 = 12 \mu\text{s}$ and $\tau_2 = 1.1$ s, and with [Mg] = 3 mol% — $\tau_1 = 2 \mu\text{s}$ and $\tau_2 = 0.1$ ms [78]. Recombination with hopping in one place (from one crystal lattice site to another) gives fast relaxation, while slow relaxation can be explained by saturation of traps, which leads to polarons („hopping“). The difference between the luminescence durations depending on the Mg concentration is due to local distortions of the crystal lattice by Mg_{Nb} defects in the LiNbO_3 ([Mg] = 7 mol%) crystal and a change in polaron conductivity [78]. In another paper [52] two distinct components of luminescence decay in the picosecond range were revealed. A change in the crystal composition (stoichiometry and/or concentration of the Mg dopant) largely affects the longer component of the luminescence duration. Thus, ($[\text{Li}]/[\text{Nb}] \approx 1$) crystal close to the stoichiometric composition and obtained by the HTSSG technology, and crystal doped with 1 mol% Mg have comparable luminescence durations. In a congruent crystal the short decay component prevails, and doping with Mg leads to increasing of the long component of the luminescence duration. The presence of both decay components is discussed by the authors on the basis of the model of self-trapped excitons [52,79]. It is proposed that the short component is due to the singlet state of excitons, which cannot migrate through the crystal lattice due to their very short intrinsic lifetime, and the long component is due to the triplet state of excitons, whose recombination is observed near defect centers.

It should be noted that the position of the matrix luminescence maximum in the visible region of the spectrum depends on the stoichiometry and state of the sample. For example, ceramics based on a mixture of Nb_2O_5 and Li_2CO_3 with an excess of the latter equal to 2 mol% show intensive luminescence in the visible region of spectrum at 440 nm at $T = 5$ K, and does not depend on the wavelength of the excitation source [59,77]. As the ambient temperature decreases, the luminescence intensity increases; at room temperature, it is almost completely quenched. With an excess of Nb_2O_5 in amount of 2 mol%, two maxima are observed in the spectrum at 440 and 520 nm, the latter being observed only upon excitation with $\lambda_{\text{ex}} = 320$ nm. In $\text{LiNbO}_{3\text{cong}}$ crystal in the polycrystalline state, only one wide luminescence band is observed at 520 nm. The maximum at 440 nm is

associated with radiative recombination between $\text{Nb}_{\text{Nb}}^{4+}$ and O^- in the main niobium octahedron, since the decay time coincides with the characteristic times for the niobium group in other connections [59]. The authors associate the maximum at 520 nm to the presence of Nb_{Li} defects with decay time $0.08 \mu\text{s}$. The paper [80] compares the photoluminescence spectrum of $\text{LiNbO}_{3\text{st}}$ crystal in the polycrystalline state with the spectrum of the crystal itself and investigates the latter intensity versus the parameters of the exciting radiation (Fig. 5, a). The difference lies only in the presence of additional radiative recombination in the long-wavelength region of the spectrum. An increase in λ_{ex} from 269 to 300 nm leads to a shift of the luminescent halo from 440 to 520 nm, which indicates the presence of two luminescence centers: $\text{Nb}_{\text{Nb}}^{4+}-\text{O}^-$ and $\text{Nb}_{\text{Li}}^{4+}-\text{O}^-$ (Fig. 5, a). Similar conclusions were obtained in the paper [53]: the stoichiometry increasing leads to shift of luminescence to the short-wavelength region of the spectrum (Fig. 5, b, c). Besides, at $\lambda_{\text{ex}} = 320$ nm, due to the greater penetrating power the luminescence is excited from the bulk of the crystal. Figure 6 shows the experimental photoluminescence spectra of the bulk and surface defects in the form of cracks, chips of crystals $\text{LiNbO}_{3\text{cong}}$, $\text{LiNbO}_{3\text{st}}$, $\text{LiNbO}_{3\text{st}}:\text{K}_2\text{O}$. It was shown in paper [81] that on the crystal surface the dominant luminescence centers at 423 and 443 nm are associated with radiative recombination between electron-hole pairs $\text{Nb}_{\text{Nb}}^{4+}-\text{O}^-$, mainly NbO_6 , since the degeneration of Nb 5d-levels may be removed due to the presence of two different distances between the central Nb ion and the surrounding oxygens (1.879 and 2.126 Å). Such feature can lead to a splitting of Nb energy levels in the crystal field of a distorted oxygen-octahedral NbO_6 cluster similar to the Jahn-Teller Fe^{2+} ion in a ligand environment in the form of O^{2-} ion octahedrons [56,82]. Besides, the change in the polarizability of NbO_6 clusters should also affect the change in the energy levels of the Nb_{Li} defects. Luminescence centers with participation of V_{Li} and Nb_{Li} point defects emit at 495 and 532 nm based on data of [80,83]. In this case, a bound small-radius polaron O^- is formed in the vicinity of the V_{Li} defect [72]. According to the model of lithium vacancies and the intensity ratio of the emission bands, the surface of $\text{LiNbO}_{3\text{cong}}$ crystal contains both defects V_{Li} and V_{Nb} , and in $\text{LiNbO}_{3\text{st}}$ crystal, there are additional inactive impurity ions in the main lithium positions, which increase the excess of V_{Li} defects [81]. Quantum-mechanical calculation of the electronic structure of lithium niobate showed that the existence of the defect in the form of a stable bipolaron pair $\text{Nb}_{\text{Nb}}^{4+}-\text{Nb}_{\text{Li}}^{4+}$ is possible, whose optical transitions are in the visible region of the spectrum at 2.3 and 2.0 eV (540 and 620 nm) [84]. The spectrum of the reconstructed LiNbO_3 crystal exhibits a wide absorption band at 2.5 eV (500 nm), which is due to the formation of the stable bipolaron pair $\text{Nb}_{\text{Nb}}^{4+}-\text{Nb}_{\text{Li}}^{4+}$ [56,85]. As the temperature increases ($T = 122-575$ K), there is a gradual thermal dissociation of bipolaron pairs into individual small-radius polarons (with repeated electron capture) $\text{Nb}_{\text{Nb}^{4+}}$ and $\text{Nb}_{\text{Li}}^{4+}$. The absorption of the latter is observed in

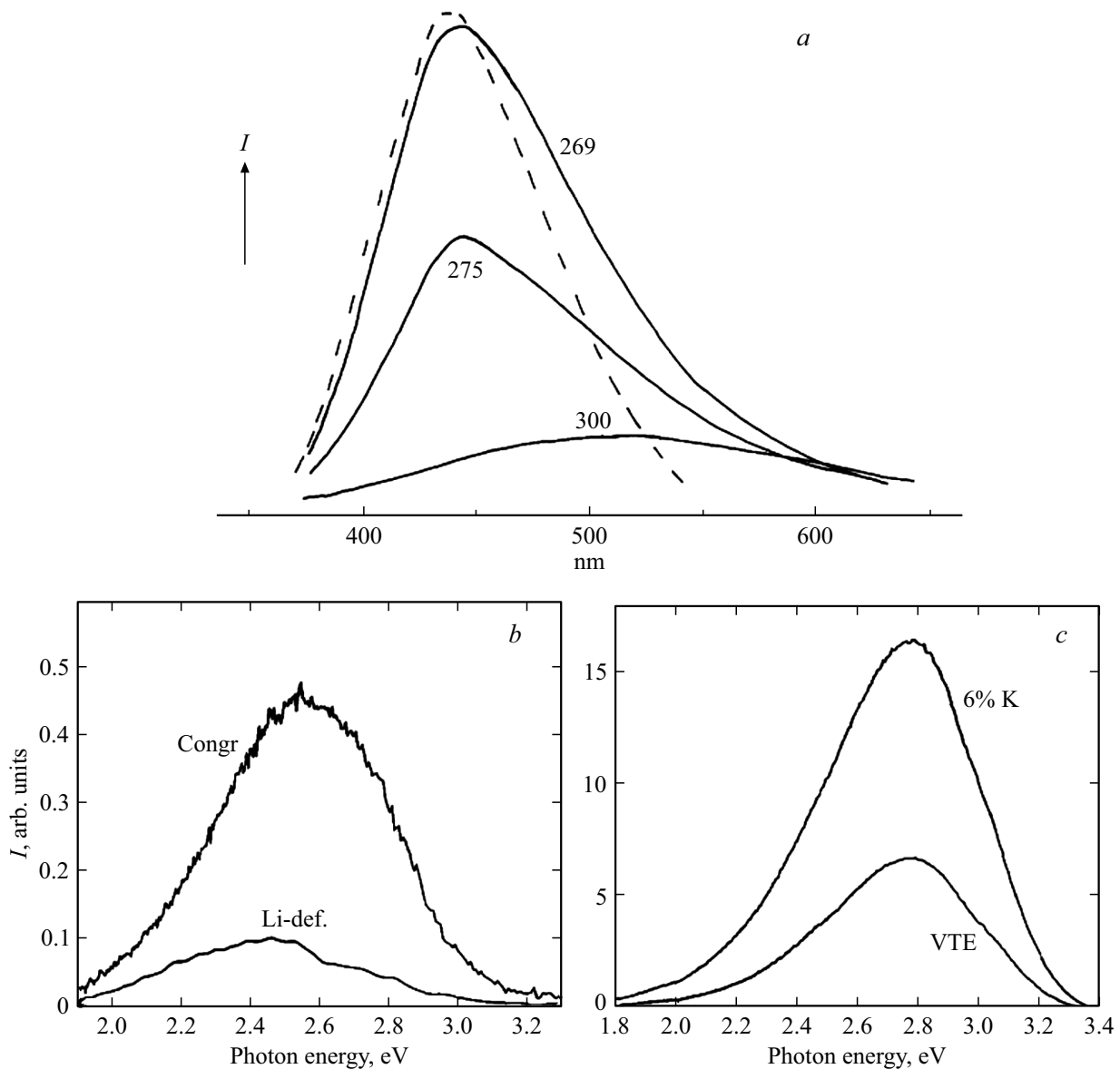


Figure 5. *a* is photoluminescence spectra of $\text{LiNbO}_{3\text{st}}$ crystal at $T = 4.2 \text{ K}$ with excitation radiation $\lambda_{\text{ex}} = 269, 275$ and 300 nm as compared with the spectrum of powdered $\text{LiNbO}_{3\text{st}}$ (dashed line) [51]; *b, c* are photoluminescence spectra of crystals $\text{LiNbO}_{3\text{cong}}$, LiNbO_3 grown from 47 mol% Li_2O (Li-def) melt, and $\text{LiNbO}_{3\text{st}}$ obtained using technology VTE (vapor transport equilibration), and crystal $\text{LiNbO}_{3\text{st}}:\text{K}_2\text{O}$ at $\lambda_{\text{ex}} = 270 \text{ nm}$ and $T = 80 \text{ K}$ [52].

the region 1.6 eV (760 nm) [85]. The role of bulk defects (Fig. 5, *b*) is described in paper [50]. Based on the literature data, the spectrum was decomposed into components in terms of point defects, which are luminescence centers, and it was found that in the bulk of $\text{LiNbO}_{3\text{cong}}$ crystal, the dominant luminescence centers are centers with the participation of Nb_{Li} defects, while in the bulk of $\text{LiNbO}_{3\text{st}}$ and $\text{LiNbO}_{3\text{st}}:\text{K}_2\text{O}$ crystals practically has no luminescence of this luminescence centers.

When luminescence was excited by X-rays in $\text{LiNbO}_{3\text{cong}}$ crystal, in contrast to the paper [59], the authors of the paper [77] observed maximum at 425 nm , which, in their opinion, is associated with the NbO_6 cluster. Besides,

very weak radiative recombination is observed at 520 nm , which is explained by the stronger penetration of X-rays into the bulk of the crystal as compared to UV radiation. Studies of cathodoluminescence in LiNbO_3 crystal after heat treatment in hydrogen at 1173 K for 45 h show three distinct maxima in the spectrum at $410, 525,$ and 580 nm , the intensity of which varies in the series of $I_{525} > I_{580} > I_{410}$. The nature of the maximum at 525 nm is compared with a strong violation of stoichiometry on the crystal surface due to desorption of Li_2O during heat treatment. Besides, intense cathodoluminescence with maximum at 800 nm in the near IR range is observed at the site of mechanical action after indentation [60].

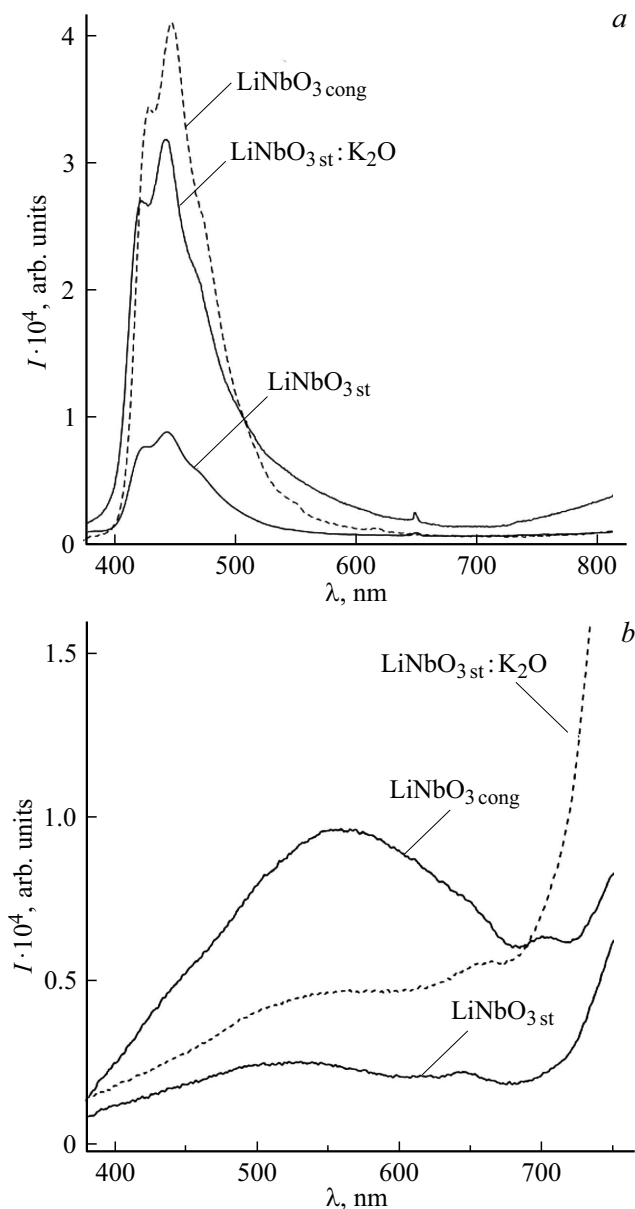


Figure 6. Photoluminescence spectra from surface (a) and bulk (b) of nominally pure LiNbO_3 crystals in the visible region of the spectrum, $\lambda_{\text{ex}} = 325 \text{ nm}$ and $T = 300 \text{ K}$.

Vacuum annealing ($> 700^\circ\text{C}$) leads to the appearance of oxygen vacancies, which are responsible for the absorption band in the visible region of the spectrum and the black color of LiNbO_3 crystal [58]. The action of radiation from a xenon lamp with a power of 150 W at 80 K on reconstructed LiNbO_3 crystal leads to a shift in the absorption maximum from 500 to 760 nm in the near IR region. This is due to the electron detachment from F -center and subsequent capture to the d -levels of Nb^{4+} . The subsequent absorption at 760 nm is due to F^+ centers. Heating to room temperature leads to „erasure“ of the absorption band at 760 nm and signal from Nb^{4+} in the EPR spectrum [54]. Irradiation with electron beam at 77 K

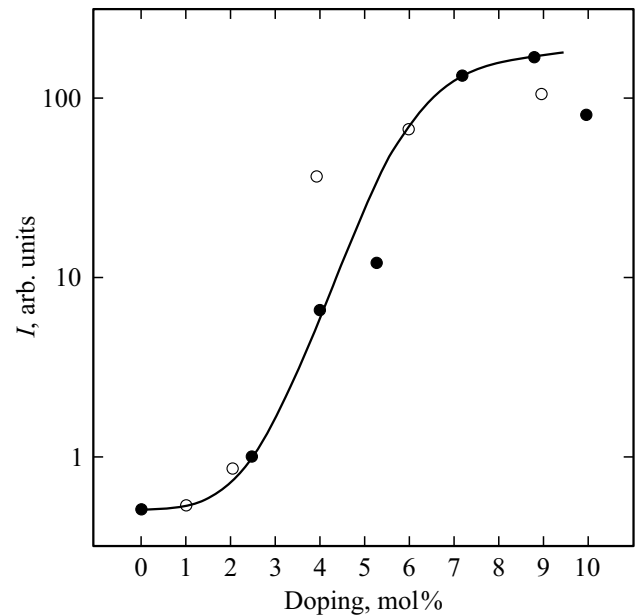


Figure 7. Integral intensity of the photoluminescence spectrum vs. dopant concentration: Zn (●) and Mg (○) at $\lambda_{\text{ex}} = 270 \text{ nm}$ and $T = 80 \text{ K}$ [52].

leads to the formation of hole traps in the form of O^- , and the absorption spectrum coincides with the absorption spectrum of F -center.

In doped $\text{LiNbO}_3:\text{Zn}$ and $\text{LiNbO}_3:\text{Mg}$ crystals the increasing of integrated luminescence intensity in the visible region is observed with increasing of dopant concentration [53,54] (Fig. 7). Decomposition of the spectra into low-energy and high-energy components with maxima at 2.3 and 2.7 eV (540 and 460 nm) made it possible to establish that as the dopant concentration increases, the intensity of the high-energy component increases, which corresponds to increased ratio $[\text{Li}]/[\text{Nb}]$ [53]. In this case, additional emission bands are not observed in the entire concentration range of dopants [53,54,86]. In our $\text{LiNbO}_3:\text{Zn}$ crystals, in similar photoluminescence spectra there are no additional emission bands at concentrations $[\text{ZnO}]_i 4.46 \text{ mol\%}$ and $[\text{MgO}]_i 5.29 \text{ mol\%}$ (Fig. 8). It was found that with the zinc concentration increasing from 0.07 to 2.01 mol% ZnO, the decreasing of the intensity of the luminescence bands due to intrinsic defects is observed due to the displacement of Nb_{Li} defects and decreasing of V_{Li} defect concentration, which indicates the increasing of $[\text{Li}]/[\text{Nb}]$ ratio. Since in our case the bulk of crystals photoluminesces, the dominant band in the high-intensity part of the spectrum is not observed. As the crystal composition approaches the second concentration threshold ($\approx 7.0 \text{ mol\% ZnO}$), the luminescent halo shifts by $\approx 0.41 \text{ eV}$ to the high-energy region of the spectrum and the intensity of luminescence centers with maxima at 2.66 and 2.26 eV (466 and 549 nm) increases due to the possible appearance of Zn_{Nb} point defects [42]. The shift effect can also be explained from the point of view of band representations of ferroelectric

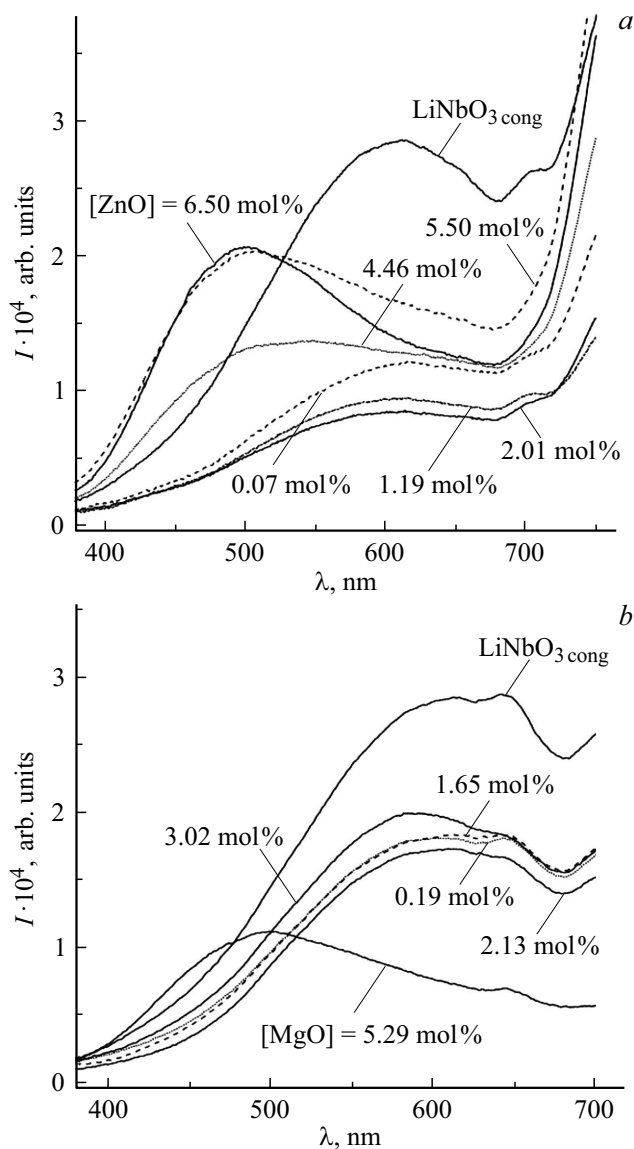


Figure 8. Photoluminescence spectra of $\text{LiNbO}_3:\text{Zn}$ (a) and $\text{LiNbO}_3:\text{Mg}$ (b) crystals in the visible region of the spectrum, $\lambda_{\text{ex}} = 325 \text{ nm}$ and $T = 300 \text{ K}$.

semiconductors [87]. As the Zn concentration increases, the concentration of Zn_{Li} defects increases, they, according to the paper [88] and our research [61], act as shallow donor energy levels. At high Zn concentrations, the energy bands near the bottom of the conduction band should be filled (the Burstein-Moss effect [89]), thereby increasing the band gap, and the luminescence spectra should undergo a „blue“ shift. Due to the similar mechanism of incorporation of Zn and Mg dopants, one can suppose a similar behavior of photoluminescence in the spectra of the crystals under study. For example, doping with Mg leads to a decrease in the intensity of radiative recombination in the visible region of the spectrum (Fig. 4) due to the incorporation into Li positions and decrease in the number of Nb_{Li} defects. At $[\text{MgO}] = 0.89 \text{ mol\%}$, the luminescent halo shifts to the

„blue“ region of the spectrum, which may indicate that the threshold value has been reached, at which Mg is incorporated into the main positions of Nb. Note that shift is observed in the near IR region of the spectrum at $[\text{ZnO}] \zeta 4.46 \text{ mol\%}$ and $[\text{MgO}] \zeta 5.29 \text{ mol\%}$ only to the long-wavelength region of the spectrum (Fig. 3).

Conclusion

Thus, due to the multifactorial effect on the luminescence properties of LiNbO_3 crystals of different composition and genesis, characterized by complex spectrum of defects, the presence in the crystal structure of distorted oxygen-octahedral clusters of various types ($\text{MeO}_6, \text{Me} = \text{Nb, Li, impurity cation}$), overlapping of the luminescence spectra from various point defects occurs. In this case, electron-phonon interactions and energy transfer occur, and the influence of the crystal field on luminescence changes. This multifactorial nature complicates the identification of luminescence centers and their nature. Undoubtedly, the luminescence in lithium niobate crystal can be divided into three regions: short-wavelength (400–500 nm) and long-wavelength (500–620 nm) regions in the visible range, and near IR region. In the short-wavelength region of the spectrum predominantly electron-hole pairs $\text{Nb}_{\text{Nb}}^{4+}-\text{O}^-$ luminesce; in long-wavelength region of spectrum the luminescence center associated with violation of stoichiometry due to the presence of Nb_{Li} and V_{Li} point defects and complex defects. The nature of polaron defects that luminesce in the near IR region of the spectrum is due to several emission centers: point defects Cr_{Nb} and Cr_{Li} in trace amounts and small radius polarons Nb_{Li} . Weak luminescence from the bulk of the crystals in the visible region of the spectrum as compared to polaron luminescence in the near IR region is due to the energy transfer between the luminescence centers. In doped $\text{LiNbO}_3:\text{Zn}$ and $\text{LiNbO}_3:\text{Mg}$ crystals, the luminescence depends on the concentration of the dopant, and as the concentration of ZnO increases to 4.46 mol% and MgO to 5.29 mol%, quenching occurs of luminescence of intrinsic defects ($\text{Nb}_{\text{Li}}, \text{V}_{\text{Li}}, \text{Nb}_{\text{Nb}}-\text{Nb}_{\text{Li}}$). The further concentration increasing of the dopant leads to shift of the luminescent halo to „blue“ region of the spectrum due to change in the mechanism of the dopant entry into the crystal lattice.

Acknowledgment

The authors express acknowledgement to V.B. Pikulev for his help in experiment on photoluminescence and discussion of experimental data.

Funding

The work was carried out under the state task of the Ministry of Science and Higher Education of the Russian Federation (theme № 0226-2018-0004, registration number AAAA-A18-118022190125-2) and with partial financial

support from the Russian Foundation for Basic Research (grant „PhD students“ № 20-33-90078).

Conflict of interest

The authors declare that they have no conflict of interest.

References

- [1] Yu.S. Kuz'minov. *Elektrooptichesky i nelineynno-optichesky kristall niobata litiya* (Nauka, M., 1987), p. 9–24 (in Russian).
- [2] M.N. Palatnikov, N.V. Sidorov, O.V. Makarova, I.V. Biryukova. *Fundamentalnye aspekty tekhnologii sil'no legirovannykh kristallov niobata litiya* (Apatity: KNTs RAN, 2017) (in Russian).
- [3] Venkatraman Gopalan, T.E. Mitchell, Y. Furukawa, K. Kitamura. *Appl. Phys. Lett.*, **72** (16), 1981 (1998). DOI: 10.1063/1.121491
- [4] N.V. Sidorov, N.A. Teplyakova, L.A. Bobreva, M.N. Palatnikov. *J. Struct. Chem.*, **60** (11), 1765 (2019). DOI: 10.1134/S002247661911009X
- [5] N.V. Sidorov, A.A. Kruk, N.A. Teplyakova, A.A. Yanichev, M.N. Palatnikov, O.Y. Pikoul. *Opt. Spectr.*, **118** (2), 259 (2015). DOI: 10.1134/S0030400X15020174
- [6] N.A. Teplyakova, N.V. Sidorov, M.N. Palatnikov. *Perspektivnye materialy*, **4**, 19 (2016) (in Russian).
- [7] Yulin Chen, Weiguo Yan, Juan Guo, Shaolin Chen, Guangyin Zhang. *Appl. Phys. Lett.*, **87** (21), 212904 (2005). DOI: 10.1063/1.2135389
- [8] S. Kumaragurubaran, S. Takekawa, M. Nakamura, S. Ganesamoorthy, K. Terabe, K. Kitamura. In: *Conference on Lasers and Electro-Optics/Quantum Electronics and Laser Science and Photonic Applications Systems Technologies, Technical Digest (CD)* (Optical Society of America, 2005), p. 393.
- [9] V.Ya. Shur, E.L. Rumyantsev, R.G. Bachko, G.D. Miller, M.M. Feyer, R.L. Bayer. *FTT*, **41** (10), 1831 (1999) (in Russian).
- [10] Donghwa Lee, Venkatraman Gopalan, S.R. Phillpot. *Appl. Phys. Lett.*, **109** (8), 082905 (2016). DOI: 10.1063/1.4961614
- [11] V. Kemlin, D. Jegouso, J. Debray, E. Boursier, P. Segonds, B. Boulanger, H. Ishizuki, T. Taira, G. Mennerat, J.-M. Melkonian, A. Godard. *Opt. Express*, **21** (23), 28886 (2013). DOI: 10.1364/OE.21.028886
- [12] Kaili Zhai, Shuanggen Zhang, Xiurong Ma, Youjian Song, Minglie Hu, Qingyue Wang, Kailiang Zhang. *IEEE Photonics J.*, **8** (2), 7802307 (2016). DOI: 10.1109/JPHOT.2016.2536364
- [13] Dong Zhou Wang, De Hui Sun, Xue Liang Kang, Yuan Hua Sang, Bo Xia Yan, Hong Liu, Yong Bi. *Opt. Express*, **23** (14), 17727 (2015). DOI: 10.1364/OE.23.017727
- [14] T.R. Volk, L.S. Kokhanchik, R.V. Gainutdinov, Y.V. Bodnarchuk, S.D. Lavrov. *J. Adv. Dielect.*, **8** (2), 1830001 (2018). DOI: 10.1142/S2010135X18300013
- [15] L. Arizmendi. *Phys. Stat. Sol. A*, **20** (2), 253 (2004). DOI: 10.1002/pssa.200303911
- [16] S.C. Abrahams, P. Marsh. *Acta Cryst.*, **B42**, 61 (1986). DOI: 10.1107/S0108768186098567
- [17] A.P. Wilkinson, A.K. Cheerham, R.H. Jarman. *J. Appl. Phys.*, **74** (5), 3080 (1993). DOI: 10.1063/1.354572
- [18] G. Dominiak-Dzik, W. Ryba-Romanowski, M.N. Palatnikov, N.V. Sidorov, V.T. Kalinnikov. *J. Mol. Struct.*, **704** (1), 139 (2004). DOI: 10.1016/j.molstruc.2004.01.063
- [19] W. Ryba-Romanowski, I. Sokolska, G. Dominiak-Dzik, S. Golab. *J. Alloys and Compounds*, **300** (2), 152 (2000). DOI: 10.1016/S0925-8388(99)00715-X
- [20] W. Ryba-Romanowski, S. Golab, G. Dominiak-Dzik, M.N. Palatnikov, N.V. Sidorov. *Appl. Phys. Lett.*, **78** (23), 3610 (2001). DOI: 10.1063/1.1376660
- [21] R. Lisiecki, B. Macalik, R. Kowalski, J. Komar, W. Ryba-Romanowski. *Crystals*, **10**—, (11), 1034 (2020). DOI: 10.3390/cryst10111034
- [22] Li Dai, Shunxiang Yang, Ruirun Chen, Chunrui Liu, Xi-anbo Han, Yu Shao. *J. Luminescence*, **217**, 116773 (2020). DOI: 10.1016/j.jlumin.2019.116773
- [23] M.N. Palatnikov, N.V. Sidorov, I.V. Biryukova, O.B. Shcherbina, V.T. Kalinnikov. *Perspektivnye materialy*, **2**, 93 (2011) (in Russian).
- [24] N.V. Sidorov, A.A. Yanichev, M.N. Palatnikov, A.A. Gabain. *Opt. Spectr.*, **116** (2), 281 (2014). DOI: 10.1134/S0030400X14010202
- [25] N.V. Sidorov, T.R. Volk, B.N. Mavrin, V.T. Kalinnikov. *Niobat litiya: defekty, fotorefraktsiya, kolebatelny spektr, polyaritony* (Nauka, M., 2003) (in Russian).
- [26] N. Zotov, H. Boysen, F. Frey, T. Metzger, E. Born. *J. Phys. Chem. Solids*, **55** (2), 145 (1994). DOI: 10.1016/0022-3697(94)90071-X
- [27] Homer Fay, W.J. Alford, H.D. Dess. *Appl. Phys. Lett.*, **12** (3), 89 (1968). DOI: 10.1063/1.1651911
- [28] P. Lerner, C. Legras, J.P. Dumas. *J. Cryst. Growth*, **3** (4), 231 (1968). DOI: 10.1016/0022-0248(68)90139-5
- [29] L. Kovacs, K. Polgar. *Cryst. Res. Technol.*, **21** (6), K101 (1986).
- [30] N. Iyi, K. Kitamura, F. Izumi, J.K. Yamamoto, T. Hayashi, H. Asano, S. Kimura. *J. Sol. Stat. Chem.*, **101** (2), 340 (1992). DOI: 10.1016/0022-4596(92)90189-3
- [31] H.J. Donnerberg, S.M. Tomlinson, C.R.A. Catlow. *J. Phys. Chem. Solids*, **52** (1), 201 (1991). DOI: 10.1016/0022-3697(91)90065-8
- [32] G.E. Peterson, A. Carnevale. *J. Chemical Physics*, **56** (10), 4848 (1972). DOI: 10.1063/1.1676960
- [33] F.P. Safaryan, R.S. Feigelson, A.M. Petrosyan. *J. Appl. Phys.*, **85** (12), 8079 (1999). DOI: 10.1063/1.370645
- [34] R.M. Araujo, K. Lengyel, R.A. Jackson, L. Kovacs, M.E.G. Valerio. *J. Phys.: Condens. Matter*, **19**, 046211 (2007). DOI: 10.1088/0953-8984/19/4/046211
- [35] F. Abdi, M.D. Fontana, M. Aillerie, P. Bourson. *Appl. Phys. A*, **83**, 427 (2006). DOI: 10.1007/s00339-006-3565-5
- [36] K. Maaidar, N. Masaif, A. Khalil. *Indian J. Phys.*, **95**, 275 (2021). DOI: 10.1007/s12648-020-01696-5
- [37] Yongfa Kong, Jingjun Xu, Xiaojun Chen, Cunzhou Zhang, Wanlin Zhang, Guangyin Zhang. *J. Appl. Phys.*, **87** (9), 4410 (2000). DOI: 10.1063/1.373085
- [38] N.V. Sidorov, B.N. Mavrin, P.G. Chufyrev, M.N. Palatnikov. *Fononnye spektry monokristallov niobata litiya* (Izdatelstvo Kol'skogo naychnogo tsentra RAN, Apatity, 2012) (in Russian).
- [39] N.V. Sidorov, N.A. Teplyakova, A.A. Yanichev, M.N. Palatnikov, O.V. Makarova, L.A. Aleshina, A.V. Kadetova. *Inorganic materials*, **53** (5), 489 (2017). DOI: 10.1134/S002016851705017X

- [40] K. Lengyel, A. Peter, L. Kovacs, G. Corradi, L. Palfavi, J. Hebling, M. Unferdorben, G. Dravecz, I. Hajdara, Zs. Szaller, K. Polgar. *Appl. Phys. Rev.*, **2** (4), 040601 (2015).
- [41] F. Abdi, M. Aillerie, M. Fontana, P. Bourson, T. Volk, B. Maximov, S. Sulyanov, N. Rubinina, M. Wohlecke. *Appl. Phys. B*, **68**, 795 (1999). DOI: 10.1007/s003409901469
- [42] T. Volk, B. Maximov, T. Chernaya, N. Rubinina, M. Wöhlecke, V. Simonov. *Appl. Phys. B*, **72** (6), 647 (2001). DOI: 10.1007/s003400100548
- [43] A.V. Kadetova. *Vliyaniye legirovaniya na strukturnye osobennosti niobata litiya*: dis. ... magistra po napravleniyu „Elektronika i nanoelektronika“ (PetrGU, Petrozavodsk, 2018) (in Russian).
- [44] J.J. Amodei, D.L. Staebler. *Appl. Phys. Lett.*, **18**, 540 (1971). DOI: 10.1063/1.1653530
- [45] D. von der Linde, A.M. Glass, K.F. Rodgers. *Appl. Phys. Lett.*, **25** (3), 155 (1974). DOI: 10.1063/1.1655420
- [46] Ye Ming, E. Kratzig, R. Orłowski. *Phys. Stat. Sol. A*, **92** (1), 221 (1985). DOI: 10.1002/pssa.2210920121
- [47] L. Tsarukyan, R. Hovsepian, R. Drampyan. *Photonics and Nanostructures — Fundamentals and Applications*, **40**, 100793 (2020). DOI: 10.1016/j.photonics.2020.100793
- [48] J.E. Midwinter, J. Warner. *J. Appl. Phys.*, **38** (2), 519 (1967). DOI: 10.1063/1.1709367
- [49] A. Hordvik, H. Schlossberg. *Appl. Phys. Lett.*, **20** (5), 197 (1972). DOI: 10.1063/1.1654106
- [50] [N.V. Sidorov, M.V. Smirnov, M.N. Palatnikov. *J. Appl. Spectrosc.*, **87** (2), 212 (2020). DOI: 10.1007/s10812-020-00986-4]
- [51] A. Harhira, L. Guilbert, P. Bourson, H. Rinnert. *Phys. Stat. Sol. C*, **4** (3), 926 (2007). DOI: 10.1002/pssc.200673755
- [52] A. Krampf, S. Messerschmidt, M. Imlau. *Scientific Reports*, **10**, 11397 (2020). DOI: 10.1038/s41598-020-68376-6
- [53] C. Fischer, M. Wöhlecke, T. Volk, N. Rubinina. *Phys. Stat. Sol. A*, **137** (1), 247 (1993). DOI: 10.1002/pssa.2211370122
- [54] F. Klose, M. Wohlecke, S. Kapphan. *Ferroelectrics*, **92** (1), 181 (1989). DOI: 10.1080/00150198908211324
- [55] T.P.J. Han, F. Jaque, V. Bermudez, E. Diefuez. *Chem. Phys. Lett.*, **369** (5–6), 519 (2003). DOI: 10.1016/S0009-2614(02)02028-6
- [56] M.G. Clark, F.J. DiSalvo, A.M. Glass, G.E. Peterson. *J. Chem. Phys.*, **59** (12), 6209 (1973). DOI: 10.1063/1.1680000
- [57] M.V. Ciampolillo, M. Bazzan, C. Sada, N. Argiolas, A. Zaltron, E. Cattaruzza, S. Mignoni, P. Bourson, M.D. Fontana, M. Bianconi. *Ferroelectrics*, **389** (1), 142 (2009). DOI: 10.1080/00150190902993275
- [58] L.E. Halliburton, K.L. Sweeney, C.Y. Chen. *Nuclear Instruments and Methods in Physics Research B*, **1** (2–3), 344 (1984). DOI: 10.1016/0168-583X(84)90090-9
- [59] D.M. Krol, G. Blasse, R.C. Powell. *J. Chem. Phys.*, **73** (1), 163 (1980). DOI: 10.1063/1.439901
- [60] J. Llopis, C. Ballesteros, R. Gonzalez, Y. Chen. *J. Appl. Phys.*, **56** (2), 460 (1984). DOI: 10.1063/1.333932
- [61] N.V. Sidorov, M.V. Smirnov, M.N. Palatnikov, V.B. Pikulev. *Opt. i spektr.*, **129** (5), 634 (2021) (in Russian). DOI: 10.21883/OS.2021.05.50891.248-20
- [62] Richard C. Powell, Edwin E. Freed. *J. Chem. Phys.*, **70** (10), 4681 (1979). DOI: 10.1063/1.437253
- [63] E.V. Stroganova. *Issledovanie, sintez i vyrashchivanie opticheskikh gradientno-aktivirovannykh kristallov na osnove niobata litiya*. Avtoref. dokt. dis. (FGBOU VO „Kubansky gosudarstvenny universitet“, Krasnodar, 2017) (in Russian). URL: <http://docspace.kubsu.ru/docspace/handle/1/1059>
- [64] V.V. Galutskii, E.V. Stroganova, N.A. Yakovenko. *Opt. Spectrosc.* **110** (3), 401 (2011). DOI: 10.1134/S0030400X10061049
- [65] V. Trepakov, A. Skvortsov, S. Kapphan, L. Jastrabik, V. Vorlíček. *Ferroelectrics*, **239** (1), 297 (2000). DOI: 10.1080/00150190008213335
- [66] P. Bourson, M. Aillerie, M. Cochez, M. Ferriol, Y. Zhang, L. Guilbert. *Optical Materials*, **24** (1–2), 111 (2003). DOI: 10.1016/S0925-3467(03)00113-7
- [67] H.-J. Reyher, R. Schulz, O. Thiemann. *Phys. Rev. B*, **50** (6), 3609 (1994). DOI: 10.1103/PhysRevB.50.3609
- [68] H. Kurz, E. Kratzig, W. Keune, H. Engelmann, U. Gonser, B. Dischler, A. Rauber. *Appl. Phys.*, **12** 355 (1977). DOI: 10.1007/BF00886038
- [69] O.F. Schirmer, D. von der Linde. *Appl. Phys. Lett.*, **33**, 35 (1978). DOI: 10.1063/1.90181
- [70] G. Blasse, A. Brill. *J. Electrochem. Soc.*, **115** (10), 1067 (1968). DOI: 10.1149/1.2410880
- [71] G. Blasse, L.G.J. De Haart. *Materials Chemistry and Physics*, **14** (5), 481 (1986). DOI: 10.1016/0254-0584(86)90050-7
- [72] O.F. Schirmer. *J. Phys.: Condens. Matter*, **18**, R667 (2006). DOI: 10.1088/0953-8984/18/43/R01
- [73] O.F. Schirmer, O. Thiemann, M. Wohlecke. *J. Phys. Chem. Solids*, **52** (1), 185 (1991). DOI: 10.1016/0022-3697(91)90064-7
- [74] P. Reichenbach, T. Kämpfe, A. Haußmann, A. Thiessen, T. Woike, R. Steudtner, L. Kocsor, Z. Szaller, L. Kovács, Lukas M. Eng. *Crystals*, **8** (5), 214 (2018). DOI: 10.3390/cryst8050214
- [75] L. Arizmendi, J.M. Cabrera, F. Agullo-Lopez. *J. Phys. C: Solid State Phys.*, **17**, 515 (1984). DOI: 10.1088/0022-3719/17/3/021
- [76] P. Reichenbach, T. Kämpfe, A. Thiessen, M. Schroder, A. Haußmann, T. Woike, L.M. Eng. *J. Appl. Phys.*, **115** (21), 213509 (2014). DOI: 10.1063/1.4881496
- [77] L. Arizmendi, J.M. Cabrera, F. Agullo-Lopez. *Solid State Commun.*, **40** (5), 583 (1981). DOI: 10.1016/0038-1098(81)90579-2
- [78] T. Kämpfe, A. Haußmann, L.M. Eng. *Phys. Rev. B*, **93** (17), 174116 (2016). DOI: 10.1103/PhysRevB.93.174116
- [79] S. Messerschmidt, A. Krampf, F. Freytag, M. Imlau, L. Vitadello, M. Bazzan, G. Corradi. *J. Phys.: Condens. Matter*, **31** (6), 065701 (2018). DOI: 10.1088/1361-648X/aaf4df
- [80] M.H.J. Emond, M. Wiegel, G. Blasse, R. Feigelson. *Mat. Res. Bull.*, **28** (10), 1025 (1993). DOI: 10.1016/0025-5408(93)90140-9
- [81] M.V. Smirnov, N.V. Sidorov, M.N. Palatnikov, V.B. Pikulev. *Trudy Kol'skogo naychnogo tsentra*, **10** (3), 323 (2019) (in Russian).
- [82] V.A. Golenishchev-Kutuzov, A.V. Golenishchev-Kutuzov, R.I. Kalimullin, A.V. Semennikov, V.A. Ulanov. *Izvestiya RAN. Seriya fizicheskaya*, **84** (12), 1754 (2020) (in Russian). DOI: 10.31857/S0367676520120212
- [83] V.Yu. Yakovlev, E.V. Kabanova, T. Weber, P. Pauffleur. *FTT*, **43** (8), 1520 (2001) (in Russian).
- [84] I.Sh. Akhmadullin, V.A. Golenishchev-Kutuzov, S.A. Migachev. *FTT*, **40** (6), 1109 (1998) (in Russian).
- [85] J. Koppitz, O.F. Schirmer, A.I. Kuznetsov. *Europhys. Lett.*, **4** (9), 1055 (1987). DOI: 10.1209/0295-5075/4/9/017

- [86] J.G. Murillo, G. Herrera, A. Vega-Rios, S. Flores-Gallardo, A. Duarte-Moller, J. Castillo-Torres. *Optical materials*, **62**, 639 (2016). DOI: 10.1016/j.optmat.2016.10.059
- [87] V.M. Fridkin. *Segnetoelektriki — poluprovodniki* (Nauka, M., 1976) (in Russian).
- [88] Yanl Li, Lili Li, Xiufeng Cheng, Xian Zhao. *J. Phys. Chem. C*, **121** (16), 8969 (2017). DOI: 10.1021/acs.jpcc.7b01274
- [89] T. Moss, G. Burrell, B. Ellis. *Poluprovodnikovaya optoelektronika*, perevod s angliyskogo A.A. Gippiusa, A.N. Kovaleva, pod red. S.A. Medvedeva. (Mir, M., 1976) (in Russian).